Supporting Information

Nitrogen and Sulfur Co-doped Carbon Dots with Strong Blue Luminescence

Hui Ding, Ji-Shi Wei, Huan-Ming Xiong*

Department of Chemistry, Fudan University, Shanghai 200433, P. R. China
E-mail: hmxiong@fudan.edu.cn

Materials. NaOH, $NaBH_4$, Na_2CO_3, K_2CO_3, $Zn(AC)_2 \cdot 2H_2O$, $SnCl_4 \cdot 5H_2O$, $Al_2(SO_4)_3$, $Cu(NO_3)_2$, $Ba(AC)_2$, $FeCl_3 \cdot 6H_2O$, $MgSO_4$, $Co(AC)_2 \cdot 4H_2O$, $FeSO_4 \cdot 7H_2O$, $CaCl_2$, $Pb(NO_3)_2$, α-lipoic acid and ethylenediamine were purchased from Sinopharm Chemical Reagent Co., Ltd (China). 3-cyclopentylpropionic acid was purchased from J&K Tech. Ltd (Beijing, China). Dulbecco's Modified Eagle's medium (DMEM, High Glucose), fetal bovine serum (FBS), and trypsinase were obtained from GIBCOBRL (New York, USA). 3-(4,5-dimethylthiazol-2-yl)-2,5-diphenyltetrazolium bromide (MTT) were obtained from Sigma Aldrich (USA). All chemical reagents were used as received without any further purification. Ultrapure water (Milli-Q water) was used in all experiments.

Instruments and characterizations. A JEM-2010 transmission electron microscope operating at 200 kV was employed to obtain high resolution transmission electron microscopy (HRTEM) images. Fluorescence spectra were recorded using a Horiba JobinYvon fluormax-4 spectrofluorometer equipped with a HORIB F-3004 sample heater/cooler Peltier thermocouple drive and an F-3018 quantum yield accessory including an integrating sphere. The UV-Vis absorption spectra were measured on a Unico UV-2802 PC spectrometer. Fourier transform infrared (FTIR) spectra were recorded on a Nicolet Nexus 470 FTIR spectrometer. The Raman spectra were recorded by a LabRam-1B microRaman spectrometer (excitation wavelength: 638.2 nm). The crystal structure of two CDs were characterized by a Bruker D8 Advance X-ray diffractometer (λ= 0.154056 nm). X-ray Photoelectron Spectroscopy (XPS) was recorded by a Perkin Elmer PHI5000C spectrometer. The time-resolved fluorospectroscopy of the sample was measured by FLS 920 spectrometer. The time-resolved transient fluorescence spectra were measured on a PTI QM 40 fluorescence lifetime spectrometer.

Principles of integrating sphere.

The detailed principles of integrating sphere are described below. When sample is placed in the integrating sphere and excited with a monochromatic light of wavelength λ, the film absorbance, *A*, is calculated by

$$A = \frac{L_b - L_c}{L_b} \qquad (1)$$

Where L_b is the integrated excitation profile when the sample is diffusely illuminated by the integrating sphere's surface; and L_c is the integrated excitation profile when the sample is directly excited by the incident beam.

The quantum yield, Φ, is by definition photons emitted to photons absorbed:

$$\Phi = \frac{E_c - (1-A)\cdot E_b}{L_a \cdot A} = \frac{E_c - E_a}{L_a - L_c} \qquad (2)$$

Where E_c is the integrated luminescence of the film caused by direct excitation, and E_b is the integrated luminescence of the film caused by indirect illumination from the sphere. The term L_a is the integrated excitation profile from an empty integrating sphere (without the sample, only a blank). Here E_a is the integrated luminescence from an empty integrating sphere (only a blank).

For integration of function *L* over the wavelength, λ, the integration limits can be from 10 nm below the excitation wavelength to 10 nm above the excitation wavelength.

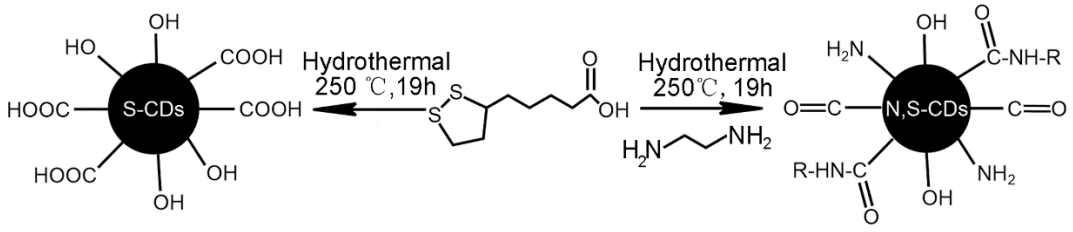

Scheme S1. Synthetic routes for S-CDs and N,S-CDs derived from α-lipoic acid.

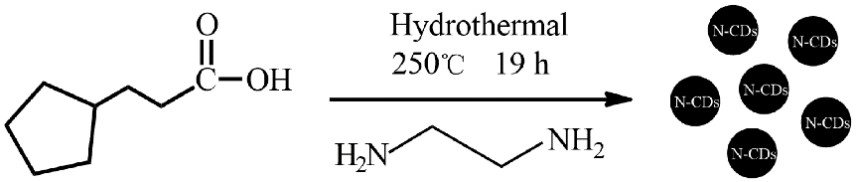

Scheme S2. Synthetic route for N-CDs derived from 3-cyclopentylpropionic acid.

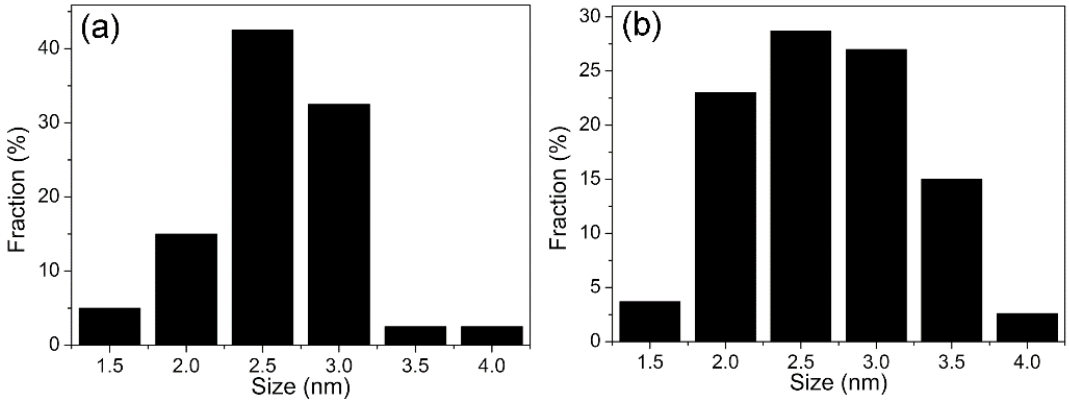

Figure S1. Size distribution histograms of the obtained (a) S-CDs and (b) N,S-CDs.

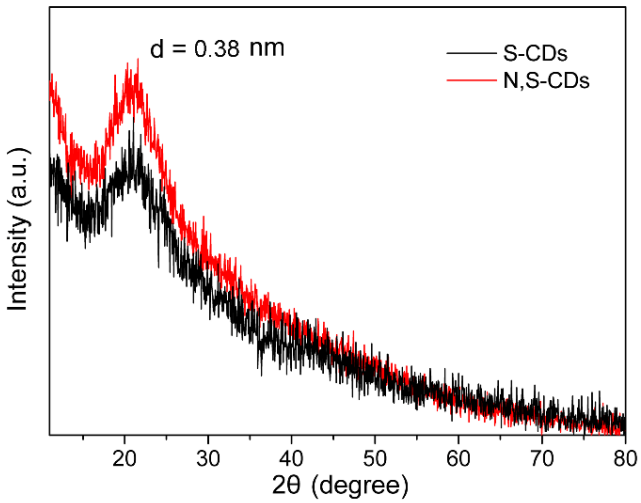

Figure S2. XRD patterns of the S-CDs and N,S-CDs.

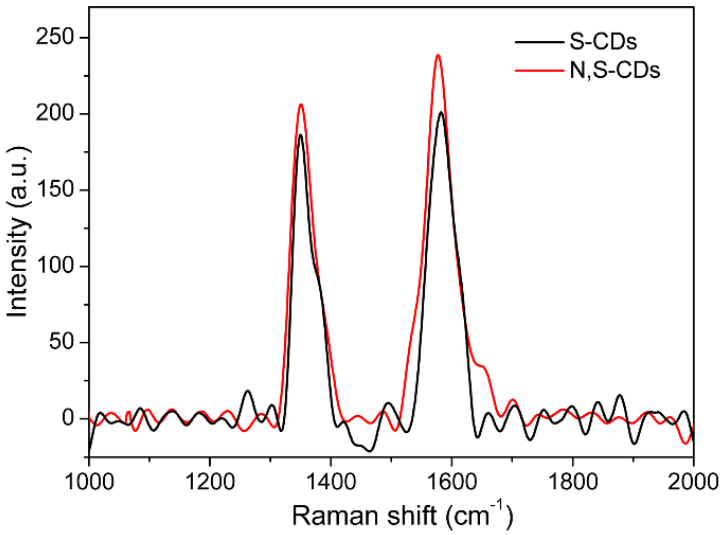

Figure S3. Raman spectra of the S-CDs and N,S-CDs.

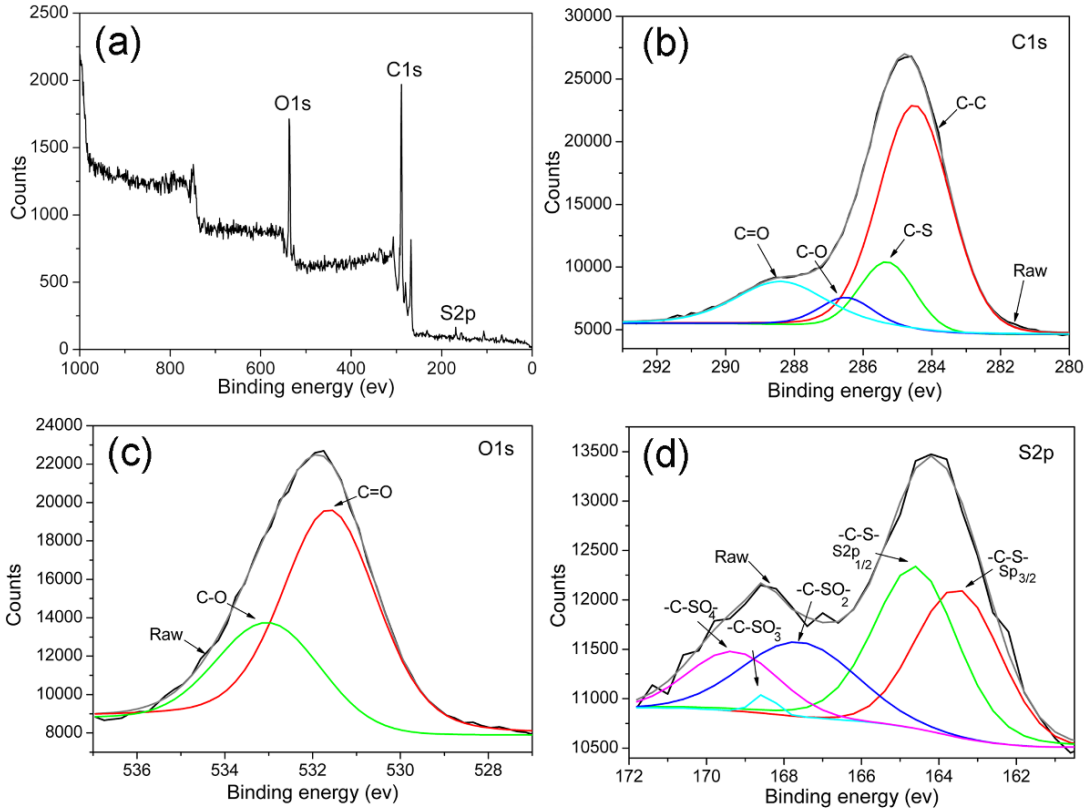

Figure S4. (a) XPS spectra of the as-prepared S-CDs. (b-d) High-resolution XPS data of C1s, N1s and S2p of S-CDs.

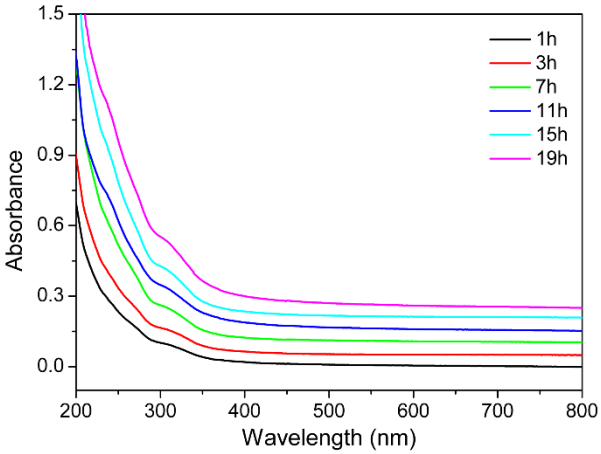

Figure S5. UV-visible absorption spectra of S-CDs respectively obtained at 250℃ for 1, 3, 7, 11, 15 and 19h.

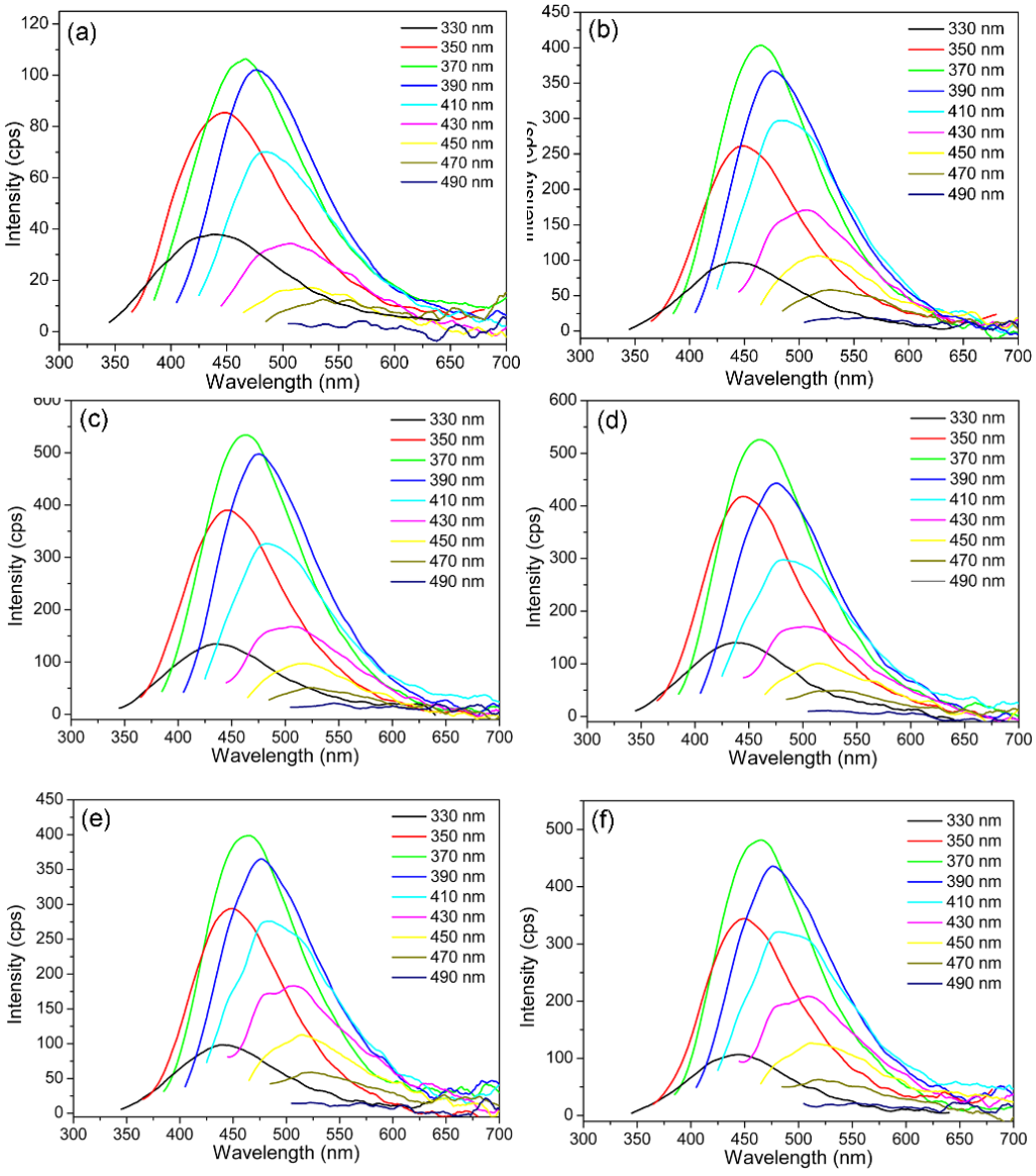

Figure S6. PL spectra of S-CDs obtained at 250℃ for 1, 3, 7, 11, 15 and 19 h

respectively. Each sample was excited by different wavelength of light.

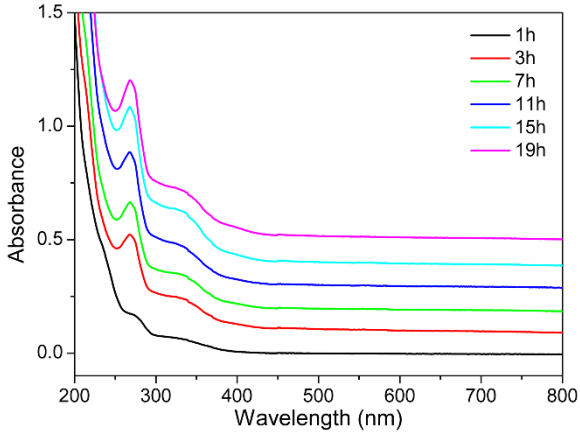

Figure S7. UV-visible spectra of N,S-CDs respectively obtained at 250℃ for 1, 3, 7, 11, 15 and 19 h.

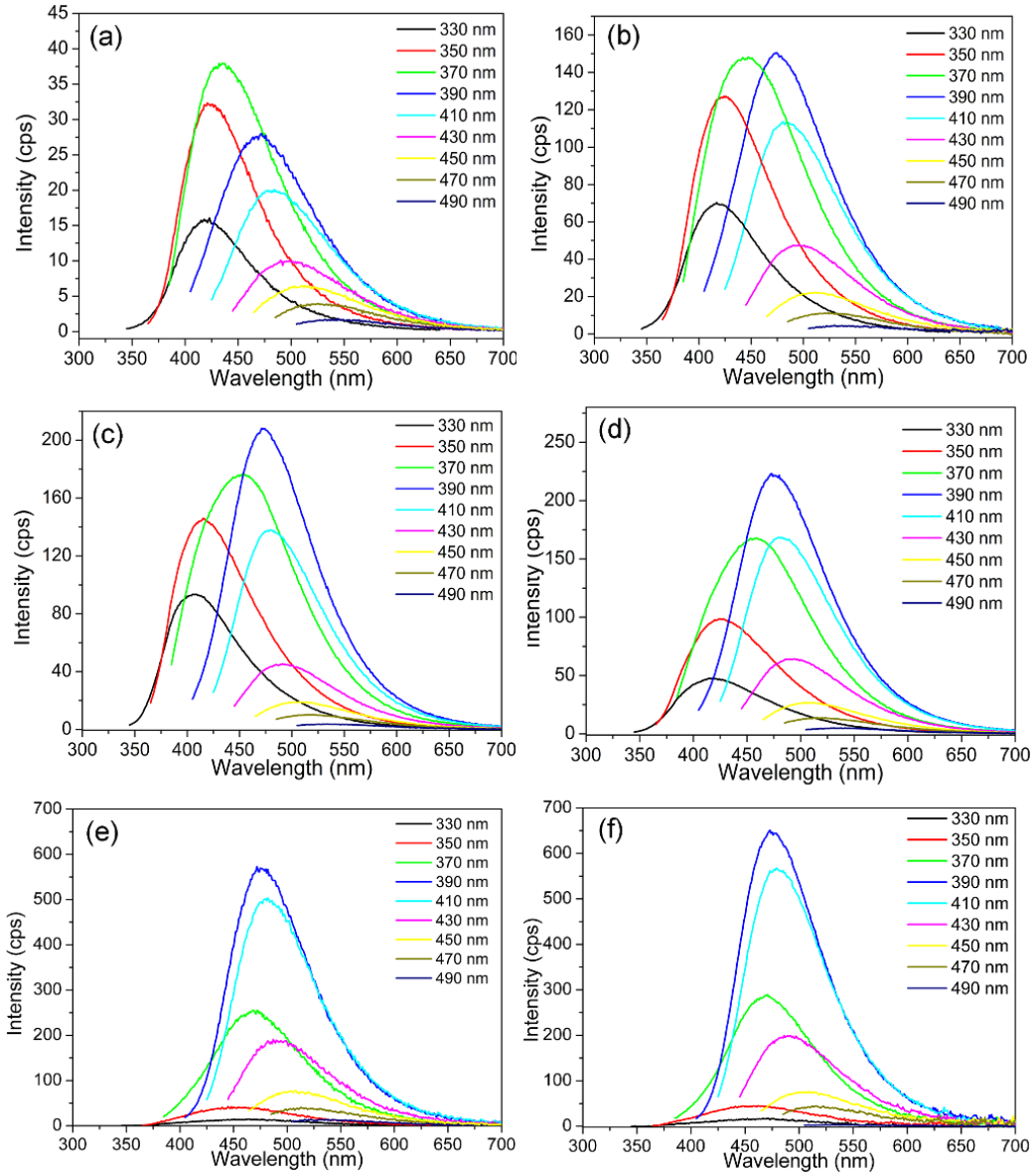

Figure S8. PL spectra of N,S-CDs obtained at 250℃ for 1, 3, 7, 11, 15 and 19 h respectively. Each sample was excited by different wavelength of light respectively.

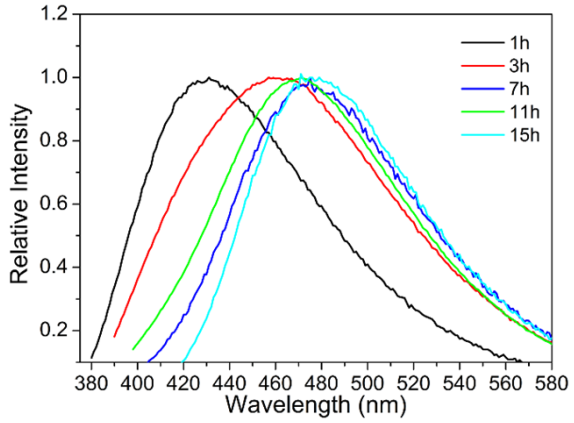

Figure S9. The normalized emission spectra of the maximal PL emission for N,S-CDs synthesized at 250℃ for different time.

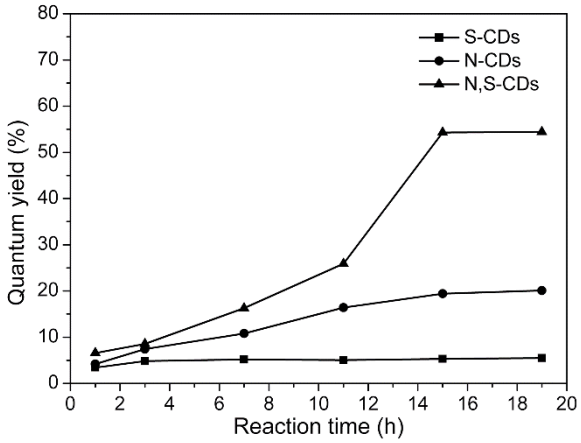

Figure S10. Quantum yield evolutions for CDs after different reaction time.

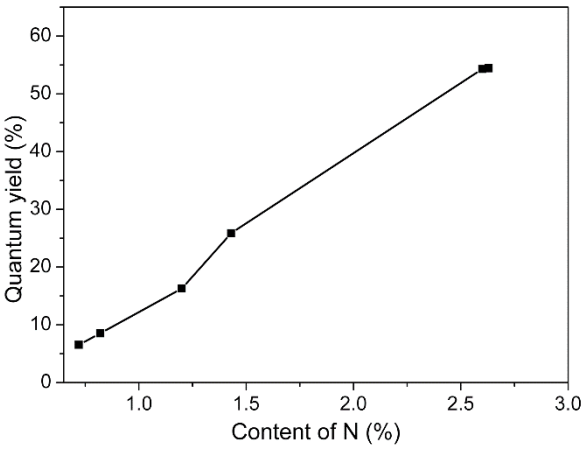

Figure S11. The relationship of quantum yield for N,S-CDs and their nitrogen

contents.

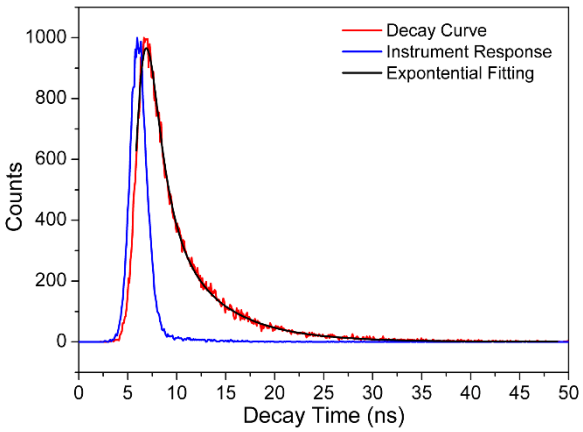

Figure S12. The fluorescence decay curve of S-CDs. The excitation and emission wavelengths are 370 and 452 nm, respectively.

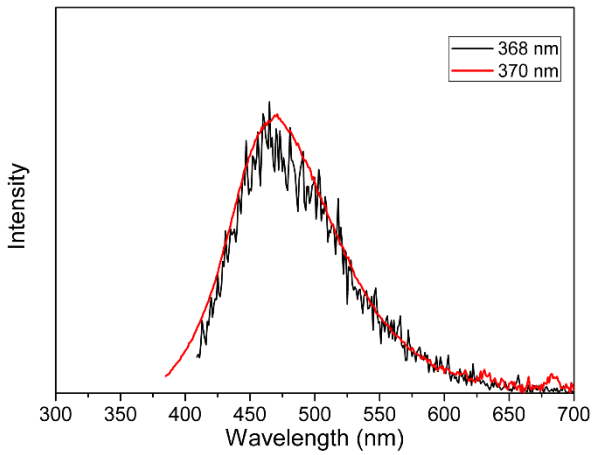

Figure S13. The red curve is the steady-state PL emission spectra of N,S-CDs excited by 370 nm light and collected by a Horiba JobinYvon fluormax-4 spectrofluorometer. The black curve is obtained by recording the transient fluorescence emission spectra of N,S-CDs excited by 368 nm light, corresponding to the τ2 of 6.54 ns, since the τ1 of 1.79 ns has passed away (see Table S3), which is recorded by a PTI QM40 fluorescence lifetime spectrometer. This result confirms that the PL emission of N,S-CDs is mainly from the luminescent process which has the lifetime of τ2.

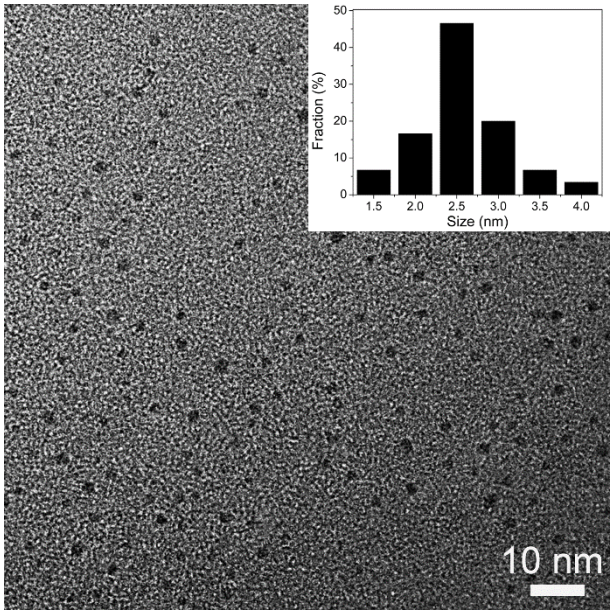

Figure S14. TEM image of the obtained N-CDs.

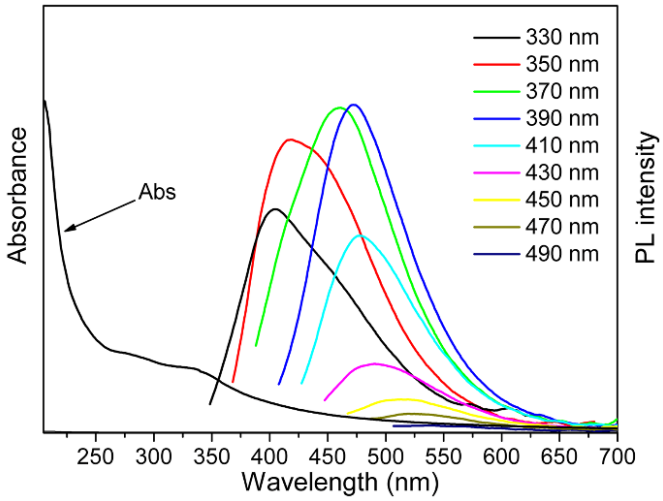

Figure S15. UV-vis absorption spectra and PL emission of N-CDs excited by different wavelength of light.

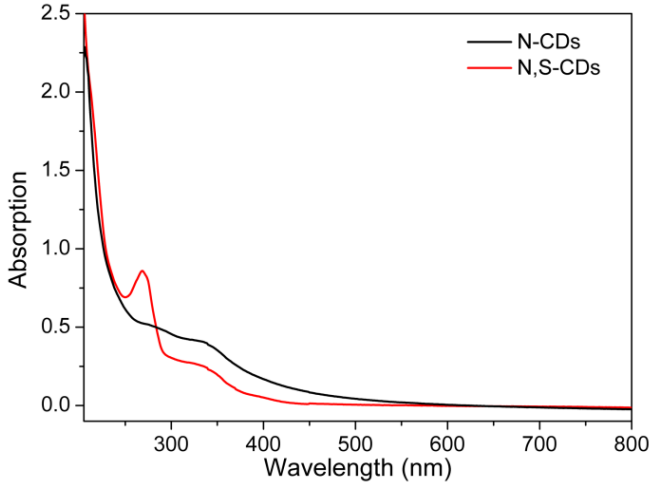

Figure S16. UV-Vis absorption spectra of N-CDs and N,S-CDs.

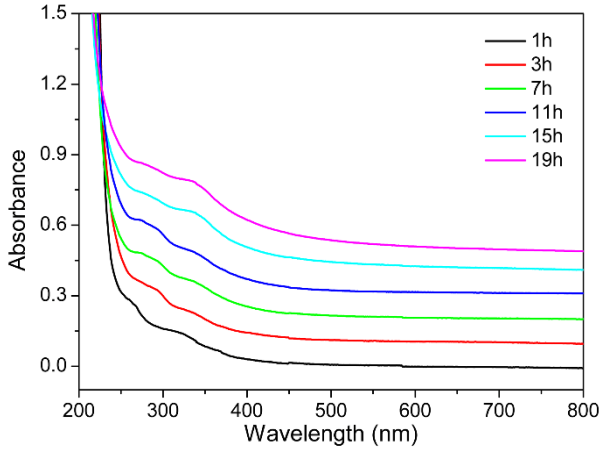

Figure S17. UV-Vis absorption spectra of N-CDs synthesized at 250℃ for 1, 3, 7, 11, 15, and 19 h respectively.

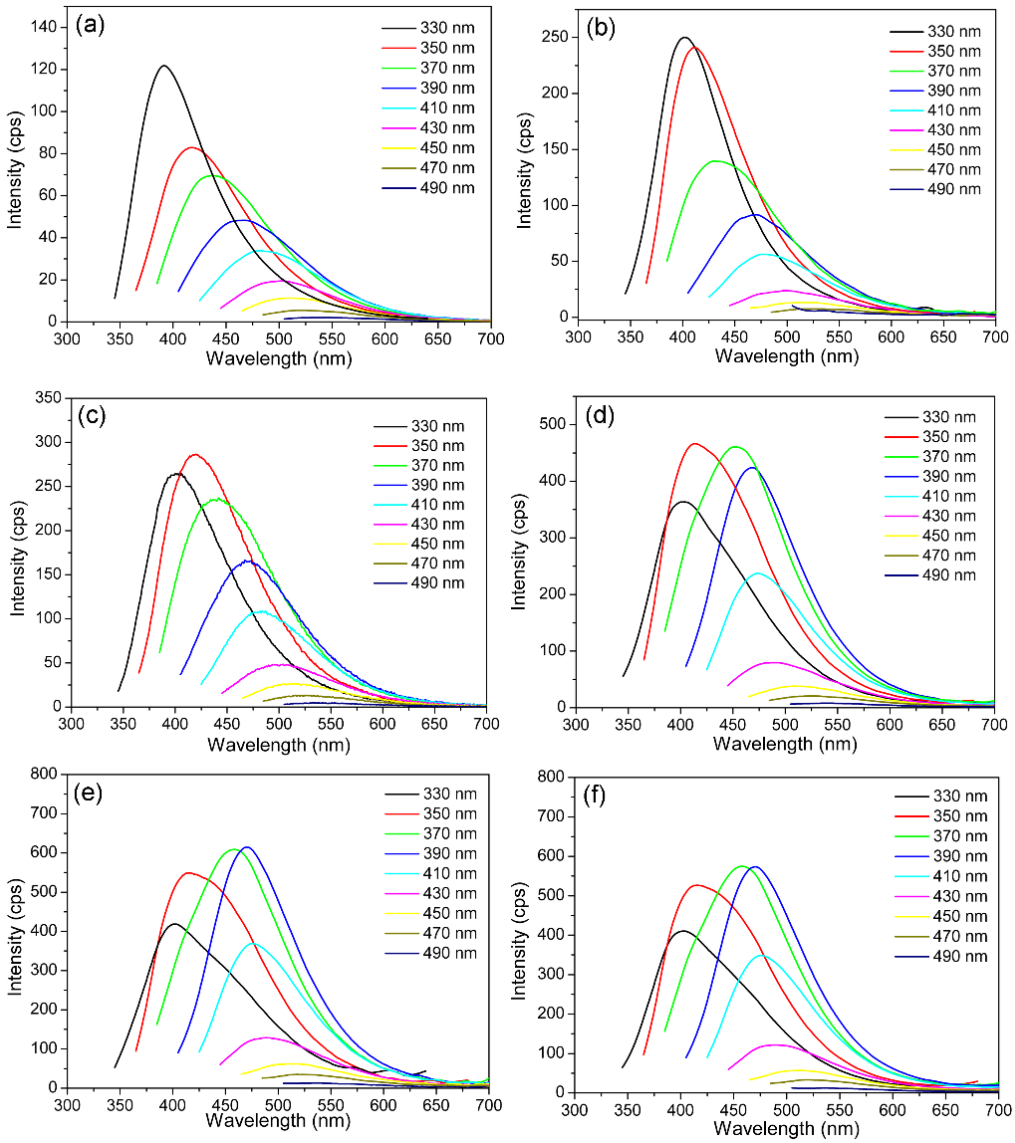

Figure S18. PL spectra of N-CDs obtained at 250℃ for 1, 3, 7, 11, 15 and 19h

respectively under different wavelength of excitation light.

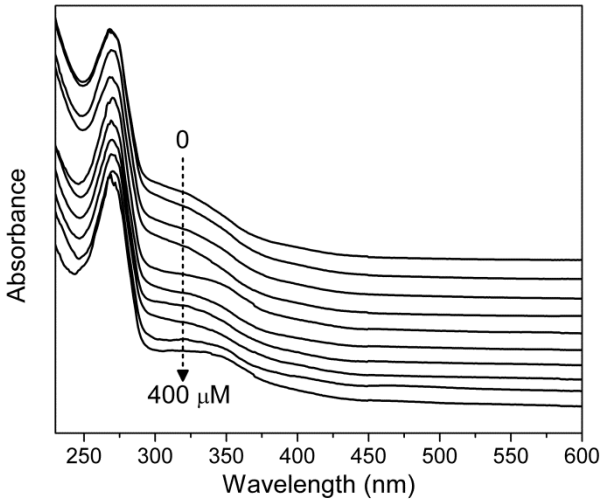

Figure S19. The UV-Vis spectra of the N,S-CDs mixed with different concentrations of Fe^{3+} in water. The absorption background of each sample is the solution containing the same concentration of Fe^{3+} ions. (The concentration of Fe^{3+} is 0, 25, 50, 75, 100, 125, 150, 200, 300, 400 μM, from top to down).

Compared with S-CDs, the most interesting finding is the observation of a new absorption peak at 270 nm in N-CDs and N,S-CDs, which may be a label to disclose the emission mechanism of CDs. In Figure S19, a decrease of absorption at 320 nm was observed upon the addition of Fe^{3+} ions, which could be attributed to the combination of Fe^{3+} ions with functional groups on the surface of N,S-CDs to form complex of N,S-CDs/Fe^{3+}. Meanwhile, the absorption peak at 270 nm shows almost no changes when more and more Fe^{3+} ions are added. The results indicates that the coordination between the C=O groups and Fe^{3+} ions decreases the C=O absorption at about 320 nm, but it does not influence the C=N bands at 270 nm which are inside the CD cores. However, we think this result is not very accurate because the absorption of Fe^{3+} ions themselves, which was used as the background to obtain Figure S19, will change actually when N,S-CDs/Fe^{3+} complex forms.

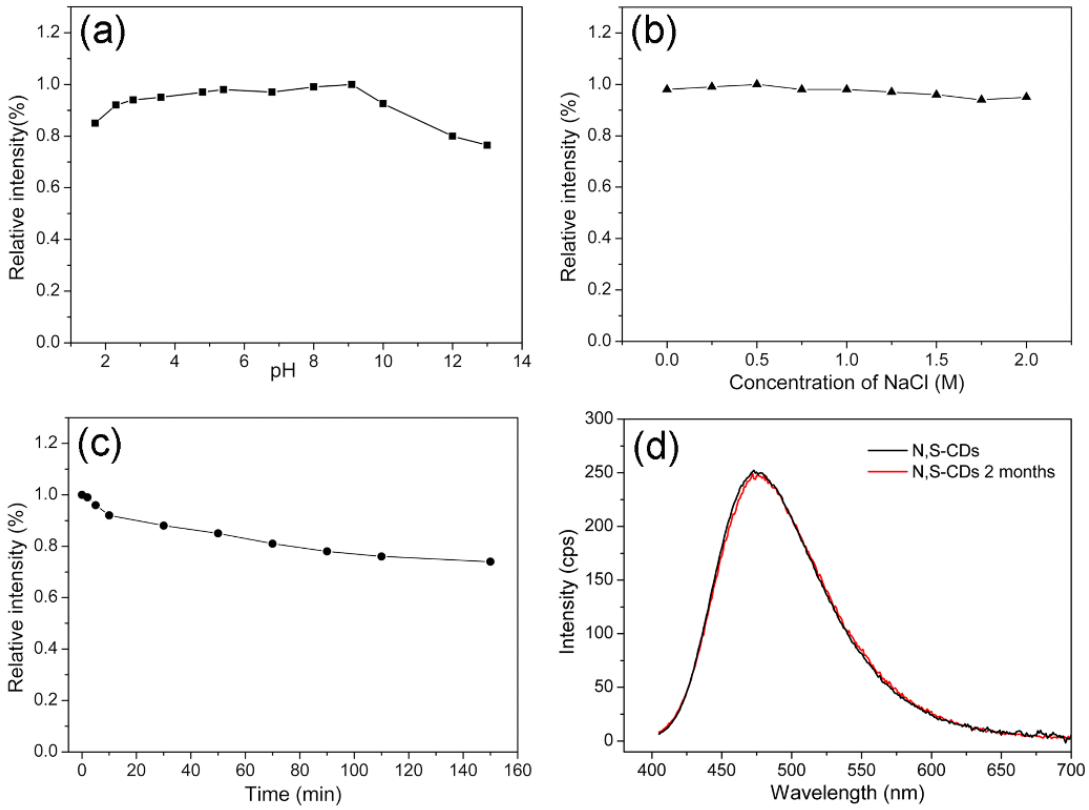

Figure S20. (a-c) Effect of pH, ionic strength and UV irradiation on the fluorescence intensity of N,S-CDs, respectively. (d) Fluorescence spectra of fresh N,S-CDs and N,S-CDs after two months of storage. All the concentrations of N,S-CDs are 100 μg/ml. The fluorescence intensities are recorded at 472 nm.

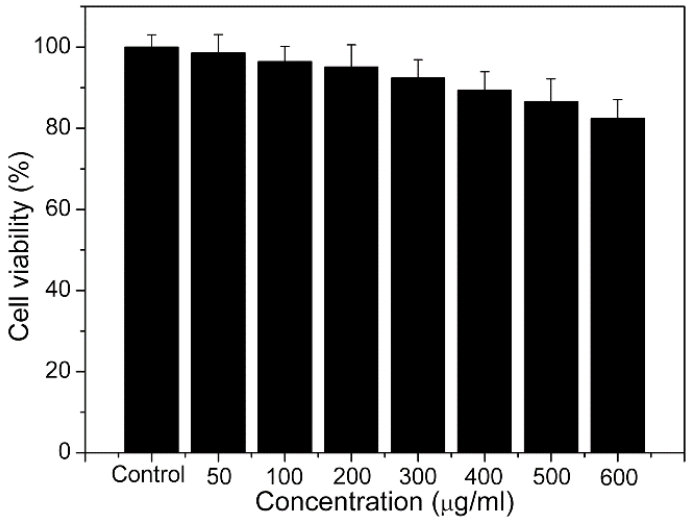

Figure S21. Cytotoxicity of the N,S-CDs toward HeLa cells from an MTT assay.

Table S1. The C, O, N and S contents of N,S-CDs synthesized at different reaction conditions.

Sample	Reaction Time (h)	C (wt %)	O (wt %)	N (wt %)	S (wt %)	Quantum Yield (%)
N,S-CDs-1h	1	75.36	19.67	0.71	0.82	6.54
N,S-CDs-3h	3	76.36	19.54	0.82	0.56	8.52
N,S-CDs-7h	7	74.89	18.78	1.20	0.38	16.28
N,S-CDs-11h	11	74.46	18.68	1.43	0.47	25.87
N,S-CDs-15h	15	73.64	18.35	2.60	1.15	54.28
N,S-CDs-19h	19	73.17	18.15	2.63	1.20	54.41

Table S2. XPS data analyses of C1s in N,S-CDs after reaction for different time.

Sample	C-C (284.5 eV) (%)	C-S (285.3 eV) (%)	C-N (286 eV) (%)	C-O (286.5 eV) (%)	C=O/C=N (288.2 eV) (%)
N,S-CDs-1h	71.33	10.37	1.26	11.30	5.74
N,S-CDs-3h	70.54	10.62	2.15	10.46	6.23
N,S-CDs-7h	69.72	10.19	2.62	9.59	7.88
N,S-CDs-11h	69.34	8.76	3.09	10.27	8.54
N,S-CDs-15h	68.29	4.80	4.31	13.56	9.04
N,S-CDs-19h	67.54	4.70	4.18	14.47	9.11

Table S3. Lifetime calculations from the time-resolved decay profiles of S-CDs and N,S-CDs.

Sample	λ_{ex} (nm)	λ_{em} (nm)	τ_1 (ns)	Percentage (%)	τ_2 (ns)	Percentage (%)	Ave.τ (ns)	χ^2
S-CDs	370	452	1.49	43.31	5.63	56.69	3.84	1.008
N,S-CDs-1h	390	472	2.10	39.40	6.91	60.60	5.01	1.003
N,S-CDs-3h	390	472	2.25	31.92	6.43	68.08	5.10	1.021
N,S-CDs-7h	390	472	1.94	20.43	6.72	79.57	5.74	1.050
N,S-CDs-11h	390	472	2.64	12.51	6.28	87.49	5.82	1.033
N,S-CDs-15h	390	472	1.95	9.62	6.63	90.38	6.18	0.991
N,S-CDs-19h	390	472	1.79	8.49	6.54	91.51	6.14	0.992